

1 **A global analysis of reconstructed land climate changes during Dansgaard-** 2 **Oeschger events**

3 Mengmeng Liu^{1,2,*}, Iain Colin Prentice¹, Sandy P. Harrison²

4 1: Georgina Mace Centre for the Living Planet, Department of Life Sciences, Imperial College
5 London, Silwood Park Campus, Buckhurst Road, Ascot SL5 7PY, UK

6 2: Department of Geography and Environmental Science, University of Reading, Reading,
7 RG6 6AB, UK

8 *** Corresponding author: m.liu18@imperial.ac.uk**

9 Ms for: *Climate of the Past*

10 **Abstract**

11 Dansgaard–Oeschger (D–O) warming events are comparable in magnitude and rate to the
12 anticipated 21st century warming. As such, they provide a good target for evaluation of the
13 ability of state-of-the-art climate models to simulate rapid climate changes. Despite the wealth
14 of qualitative information about climate changes during the D–O events, there has been no
15 attempt to date to make quantitative reconstructions globally. Here we provide reconstructions
16 of seasonal temperature changes and changes in plant-available moisture across multiple D–O
17 events during Marine Isotope Stage 3 based on available pollen records across the globe. These
18 reconstructions show that the largest warming occurred in northern extratropics, especially
19 Eurasia, while western North America and the southern extratropics were characterised by
20 cooling. The change in winter temperature was significantly larger than the change in summer
21 temperature in the northern extratropics, indicating that the D–O warming events were
22 characterised by reduced seasonality, but there is no significant difference between the summer
23 and winter temperature changes in the southern extratropics. The antiphasing between northern
24 and southern extratropical changes, and the west-east pattern of cooling and warming in North
25 America are consistent across the eight D–O events examined, although the signal at individual
26 sites may vary between events. These reconstructions show that the largest changes in
27 temperature occurred in northern extratropics, especially Europe and Eurasia. The change in
28 winter temperature was not significantly different from the change in summer temperature, and
29 thus there is no evidence that the D–O events were characterised by a change in seasonality.

30 ~~Although broadscale features of the temperature changes were consistent across the eight D-O~~
31 ~~events examined, the spatial patterns of temperature changes vary between events.~~ Globally,
32 changes in moisture were positively correlated with changes in temperature, but the strength
33 and the sign of this relationship vary regionally. These reconstructions can be used to evaluate
34 the spatial patterns of changes in temperature and moisture in the transient simulations of the
35 D-O events planned as part of the Palaeoclimate Modelling Intercomparison Project.

36 1. Introduction

37 Dansgaard–Oeschger (D–O) events are characterised in Greenland by a transition from cold
38 Greenland Stadial (GS) to warmer Greenland Interstadial (GI) conditions (Dansgaard et al.,
39 1993). The surface air temperature in Greenland increased by 10–15° C during the warming
40 phases; these warming events occur over an interval of between 50 and 200 years (Huber et
41 al., 2006; Kindler et al., 2014). Thus, the D-O events offer a parallel in terms of speed to
42 projected future warming, although both the baseline state and the mechanism inducing this
43 warming differ from anticipated 21st century climate changes. D-O events could therefore
44 provide an opportunity to determine how well climate models that are used for future
45 projections can simulate rapid climate changes (Malmierca-Vallet et al., 2023), particularly
46 regional patterns of warming (and cooling) that are regarded as a challenge for modelling
47 (Doblas-Reyes et al., 2021; Lee et al., 2021) and are highly important in assessing the
48 vulnerability of human societies to future climate changes (IPCC 2022).

49 ~~Thus, the D-O events offer a parallel in terms of speed to projected future warming, although~~
50 ~~both the baseline state and the mechanism inducing this warming differ from anticipated 21st~~
51 ~~century climate changes. D-O events could therefore provide an opportunity to determine how~~
52 ~~well climate models that are used for future projections can simulate rapid climate changes~~
53 ~~(Malmierca-Vallet et al., 2023).~~

54 D-O events are registered globally (Voelker, 2002; Sánchez Goñi and Harrison, 2010; Harrison
55 and Sánchez Goñi, 2010; Sánchez Goñi et al., 2017; Adolphi et al., 2019; Corrick et al., 2020).
56 Shifts in vegetation types between GI and GS states have been interpreted as primarily a
57 temperature signal in the extratropics and a moisture signal in the tropics (Harrison and
58 Sánchez Goñi, 2010). Speleothem records provide a good time-control on the synchronicity of
59 climate changes globally with the D-O events registered in Greenland (Adolphi et al., 2019;
60 Corrick et al., 2020), but the driver of this signal can either be temperature or precipitation
61 depending on the region. There are quantitative climate reconstructions based on terrestrial
62 pollen records from La Grande Pile (Guiot et al., 1993), Lago Grande di Monticchio (Huntley
63 et al., 1999), Padul (Camuera et al., 2022), El Cañizar de Villarquemado (Wei et al., 2021;
64 Camuera et al., 2022) and Lake Ohrid (Sinopoli et al., 2019), marine cores in the western
65 Mediterranean and offshore from Portugal (Sánchez-Goñi et al., 2002), diatom assemblages at
66 Les Echets, France (Ampel et al., 2010), bacterial membrane lipid records from the Eifel region

67 ~~(Zander et al., 2023), isotopic measurements of earthworm calcite from the Rhine Valley~~
68 ~~(Prud'homme et al., 2022) and clumped isotope measurements on snails in Hungary (Újvári et~~
69 ~~al., 2021). There are quantitative climate reconstructions based on pollen records from La~~
70 ~~Grande Pile (Guiot et al., 1993), Lago Grande di Monticchio (Huntley et al., 1999), Padul~~
71 ~~(Camuera et al., 2022), El Cañizar de Villarquemado (Wei et al., 2021; Camuera et al., 2022)~~
72 ~~and Lake Ohrid (Sinopoli et al., 2019), diatom assemblages at Les Echets, France (Ampel et~~
73 ~~al., 2010), bacterial membrane lipid records from the Eifel region (Zander et al., 2023), isotopic~~
74 ~~measurements of earthworm calcite from the Rhine Valley (Prud'homme et al., 2022) and~~
75 ~~clumped isotope measurements on snails in Hungary (Újvári et al., 2021).~~ Aside from the lack
76 of comparable quantitative estimates from outside Europe, differences in the methodology
77 employed and in the specific climate variables reconstructed in each of these studies limits
78 their usefulness for model evaluation. In particular, given that there is still uncertainty as to
79 whether the D-O cycles are characterised by changes in seasonality such that warming events
80 are primarily driven by changes in winter (Flückiger et al., 2008; ~~Zander et al., 2023~~[Zander et](#)
81 [al., 2024](#)), in the regional strength of the warming (Harrison and Sánchez Goñi, 2010) and how
82 warming relates to changes in moisture (Wei et al., 2021), there is a need for more systematic
83 reconstruction of seasonal climate changes.

84 ~~In the paper, we provide reconstructions of seasonal temperature changes and changes in plant-~~
85 ~~available moisture during the intervals corresponding to D-O warming events in Greenland~~
86 ~~during Marine Isotope Stage 3 based on available pollen records globally. In the paper, we~~
87 ~~provide reconstructions of seasonal temperature changes and changes in plant available~~
88 ~~moisture across multiple D-O events during Marine Isotope Stage 3 based on available pollen~~
89 ~~records globally.~~ We employ a standard methodology to construct age models for these records,
90 as well as a standard regression-based approach to make the reconstructions. We analyse the
91 regional patterns to identify key targets for model evaluation.

92 **2. Methods**

93 **2.1. Data sources**

94 Modern pollen data were obtained from version 2 of the SPECIAL Modern Pollen Data Set
95 (SMPDSv2: Villegas-Diaz and Harrison, 2022). This global data set contains 24649 modern
96 pollen records from 17827 sites. The dataset contains relative abundance records for 4816
97 pollen taxa, created after removing taxa that are not climatically diagnostic (e.g. obligate

98 aquatics, carnivorous species, cultivated plants). The data set provides several levels of
99 taxonomic aggregation; here we use the most aggregated level, where woody species were
100 generally combined at genus level and herbaceous species at sub-family or family level unless
101 they were palynologically distinctive, occupied distinctive ecological niches and were
102 sufficiently geographically widespread. This "amalgamated" data set contains relative
103 abundance information for 1338 taxa. These samples were aggregated by longitude, latitude
104 and elevation in order to remove duplicates. Counts for *Quercus*, *Quercus* (deciduous) and
105 *Quercus* (evergreen) were combined because of inconsistent differentiation of *Quercus* pollen
106 in different regional records. Deciduous and evergreen oaks occupy different areas of climate
107 space, particularly in terms of seasonal moisture; specifically, evergreen oaks are typically
108 found in areas characterised by winter rainfall such as the Mediterranean. Nevertheless, since
109 there are other plant taxa that are similarly diagnostic of such regimes, the amalgamation of
110 *Quercus* (deciduous) and *Quercus* (evergreen) should not have a major effect on the robustness
111 of our climate reconstructions. Counts for *Quercus*, *Quercus* (deciduous) and *Quercus*
112 (evergreen) were combined because of inconsistent differentiation of *Quercus* pollen in
113 different regional records. Taxa that occurred in less than 10 samples in the training data set
114 were not used to make reconstructions because it is unlikely that the available samples provided
115 a reasonable estimate of the climate space occupied by these rare taxa (Liu et al., 2020). After
116 filtering, the data set contains information on 591 individual pollen taxa from 17547 sites
117 (Figure 1).

118 ~~Taxa with <10 occurrences were removed to avoid the problem of rarity (Liu et al., 2020).~~
119 ~~After this filtering, the data set contains 17547 sites (Figure 1) with 591 taxa.~~

120 The SMPDSv2 also provides climatic information at each pollen site, specifically the mean
121 temperature of the coldest month (MTCO), mean temperature of the warmest month (MTWA),
122 and a moisture index (α) calculated as the ratio of actual evapotranspiration to equilibrium
123 evapotranspiration. These bioclimate variables reflect mechanistically distinct controls on
124 plant growth.

125 The fossil pollen data were obtained from the Abrupt Climate Changes and Environmental
126 Responses (ACER) database (Sánchez Goñi et al., 2017), which includes 93 records from the
127 last glacial period (73-15 ka) with sufficient resolution and dating control to detect sub-
128 millennial scale variability. Here we focus on the 73 records covering most of Marine Isotope

129 Stage 3 (50-30 ka); 54 of these records are from terrestrial sites and 19 from ~~continental-shelf~~
130 marine sites (Figure 1; Table 1). The fossil data were taxonomically harmonised to be
131 consistent with the SMPDSv2.

132 2.2. Climate reconstruction method

133 We used tolerance-weighted Weighted Averaging Partial Least Squares (*fx*TWA-PLS: Liu et
134 al., 2020; Liu et al., 2023) regression to model the relationships between taxon abundances and
135 individual climate variables in the SMPDSv2 modern training dataset and then applied these
136 relationships to reconstruct past climate using the fossil assemblages from the ACER database
137 (Figure 2). *fx*TWA-PLS reduces the tendency of regression methods to compress
138 reconstructions towards the centre of the sampled climate range by applying a sampling
139 frequency correction to reduce the influence of uneven sampling of climate space and
140 weighting the contribution of individual taxa according to their climate tolerances (Liu et al.,
141 2020). Version 2 of *fx*TWA-PLS (*fx*TWA-PLS2, Liu et al., 2023) uses P-splines smoothing to
142 derive the frequency correction and applies this correction both in estimating the climate
143 optima and tolerances, and in the regression itself, producing a further improvement in model
144 performance compared to version 1 (Liu et al., 2020).

145 We evaluated the *fx*TWA-PLS models by comparing the reconstructions with observations
146 using leave-out cross-validation, where one site at a time was randomly selected as a test site
147 and sites that are both geographically close (within 50 km horizontal distance from the site)
148 and climatically close (within 2% of the full range of each climate variable in the dataset) were
149 removed from the training set along with this test site, to prevent redundancy in the climate
150 information from inflating the cross-validation goodness of fit, following Liu et al. (2020).
151 ~~where one site at a time was randomly selected as a test site and geographically and climatically~~
152 ~~similar sites were removed from the training set to prevent redundancy in the climate~~
153 ~~information from inflating the cross-validation goodness of fit.~~ We selected the last significant
154 number of components (p -value ≤ 0.01) and assessed model performance using the root mean
155 square error of prediction (RMSEP). Compression was assessed using linear regression of the
156 leave-out cross-validated reconstructions on to the climate and local compression was assessed
157 by loess regression (*loefit*). Reconstructions variable. Reconstructions of MTCO, MTWA and
158 α were made for every sample in each fossil record. Sample specific errors were estimated via
159 bootstrapping, as described in Liu et al. (2020). We corrected for the effect of changes in

160 atmospheric CO₂ on plant water-use efficiency, and hence the reconstructions of α (Figure S1),
161 following Prentice et al. (2022). Appropriate values of CO₂ were taken from the WAIS Divide
162 ice core record (Bauska et al., 2021).

163 2.3. Age modelling

164 ~~Although the ACER database provides age models for each pollen record, the resolution of the~~
165 ~~individual records is variable (mean resolution 474 years) and these models are often~~
166 ~~imperfectly aligned with the dating of D-O events as recorded in the Greenland ice core. To~~
167 ~~create a better alignment, we used dynamic time warping (DTW: Belman and Kalaba, 1959;~~
168 ~~Burstyn et al., 2021) to adjust the age scale for each individual record (Figure 2). Dynamic~~
169 ~~time warping optimises the similarity between two sequences by stretching or compressing one~~
170 ~~sequence in the time dimension to match the other. Here, we use simulated mean annual~~
171 ~~temperature from a transient simulation of the interval 50-30 ka made with the LOVECLIM~~
172 ~~model (Menviel et al., 2014) as the reference sequence. We used the mid point between the~~
173 ~~start dates of each D-O event (Wolff et al., 2010; converted into AICC2012 timescale) to sub-~~
174 ~~divide each record into discrete intervals. For each site in each interval, we modify the time~~
175 ~~scale of the reconstructed mean annual temperature series in each ACER record to match the~~
176 ~~reference, after having normalised both sequences to remove the influence of differences in~~
177 ~~absolute values and the amplitude of changes. To remove the influence of the variable temporal~~
178 ~~resolution of the pollen records we interpolated the reconstructions from individual samples to~~
179 ~~provide estimates at regular intervals (25 years) through each record. The adjusted age model~~
180 ~~for each site was then applied to the reconstructions of MTCO, MTWA, and α for that~~
181 ~~site.~~Although the ACER database provides age models for each pollen record, the resolution
182 of the individual records is variable (mean resolution 474 years) and these models are often
183 imperfectly aligned with the dating of D-O events as recorded in the Greenland ice core, and
184 which have been shown to have a globally synchronous imprint through analysis of speleothem
185 records (Adolphi et al., 2019; Corrick et al., 2020). To create a better alignment, we used
186 dynamic time warping (DTW: Belman and Kalaba, 1959; Burstyn et al., 2021) to adjust the
187 age scale for each individual record (Figure 2). Dynamic time warping optimises the similarity
188 between two sequences by stretching or compressing one sequence in the time dimension to
189 match the other. Here, we use simulated mean annual temperature (MAT) from a transient
190 simulation of the interval 50-30 ka made with the LOVECLIM model (Menviel et al., 2014)
191 as the reference sequence comparedaring to MAT calculated as the average of MTCO and

192 MTWA from the individual pollen records. We used the mid-point between the start dates of
 193 each D-O event (Wolff et al., 2010; converted into AICC2012 timescale) to sub-divide each
 194 ACER record into discrete intervals and modified the time scale of the reconstructed mean
 195 annual temperature series in each interval to match the reference sequence, having normalised
 196 both sequences to remove the influence of differences in absolute values and the amplitude of
 197 changes. The adjusted age model for each ACER record was then applied to the reconstructions
 198 of MTCO, MTWA, and α from that record for subsequent analyses.

199 2.4. Assessment of regional climate changes during Greenland D-O warming events

200 ~~2.4. Assessment of changes during D-O events~~

201 ~~To estimate the magnitude of climate changes over the D-O events, we used a third-order~~
 202 ~~polynomial to fit the reconstructions during the interval from 300 years before to 600 years~~
 203 ~~after the official start date of each event (Wolff et al., 2010; converted into AICC2012~~
 204 ~~timescale) to obtain the sign of changes (increase or decrease). We used the ages corresponding~~
 205 ~~to the minimum and maximum in the fitted polynomial ($t_{\min \text{ polynomial}}$, $t_{\max \text{ polynomial}}$) but, since~~
 206 ~~the smoothed polynomial may underestimate the amplitude of change, we used the~~
 207 ~~reconstructed minimum or maximum value within the period $t_{\min \text{ polynomial}} \pm 100$ years or t_{\max~~
 208 ~~$\text{polynomial}} \pm 100$ years respectively. The magnitude of climate change during the interval~~
 209 ~~corresponding to each D-O warming event as registered in Greenland is calculated individually~~
 210 ~~for each climate variable at each site. To avoid making an assumption about the sign of the~~
 211 ~~climate change at a site, we used a third-order polynomial to fit the reconstructions during the~~
 212 ~~interval from 300 years before to 600 years after the official start date of each event (Wolff et~~
 213 ~~al., 2010; converted into AICC2012 timescale) to determine whether the change was positive~~
 214 ~~or negative. We used the ages corresponding to the minimum and maximum in the fitted~~
 215 ~~polynomial ($t_{\min \text{ polynomial}}$, $t_{\max \text{ polynomial}}$). However, since the smoothed polynomial may~~
 216 ~~underestimate or overestimate the amplitude of change, we used the reconstructed minimum~~
 217 ~~or maximum value within the period $t_{\min \text{ polynomial}} \pm 100$ years or $t_{\max \text{ polynomial}} \pm 100$ years~~
 218 ~~respectively (see Figure S2).~~

219 In cases where no change was registered for all of the three climate variables, we assume that
 220 the event was not registered at the site. As a measure of the accuracy of the DTW method to
 221 identify D-O events, we compared the number of identified events with the number of D-O
 222 events that occurred during the time covered by each record (Table 1). To assess whether events

223 were missed in a particular record due to low sampling resolution, we examined the number of
 224 samples present in the 900-year interval covering the sampled D-O (i.e. 300 years before to
 225 600 years after the official start date of each event), where low resolution was defined as ≤ 3
 226 samples in this 900-year interval. Reconstructions covering intervals where a signal was not
 227 identified were not used in subsequent analyses.

228 We calculated sample-specific errors for the minimum and maximum reconstructed values.
 229 Assuming that the minimum and maximum values are independent, we used error propagation
 230 to obtain the error of the change:

$$231 \quad \sigma_{change} = \sqrt{\sigma_{min}^2 + \sigma_{max}^2}$$

232 Following Liu et al. (2022), we used a maximum likelihood method to estimate the ratio of
 233 Δ MTCO to Δ MTWA (and ratio of $\Delta\alpha$ to Δ MTWA) to take account of the errors on both
 234 variables.

235 **3. Results**

236 *fx*TWA-PLS reproduces the modern climate reasonably well (Table 2). The performance is
 237 best for MTCO (R^2 0.75, RMSEP 6.51, slope 0.85) but is also good for MTWA (R^2 0.59,
 238 RMSEP 3.68, slope 0.71) and α (R^2 0.65, RMSEP 0.18, slope 0.71). Assessment of the variance
 239 inflation factor scores shows that there is no problem of multicollinearity so that it is possible
 240 to reconstruct all three climate variables independently (Liu et al., 2023).

241 The use of dynamic time-warping made it possible to identify D-O events robustly (Table 1;
 242 Supplementary Table 1). Thirteen of the 73 sites cover some part of the 50-30 ka periods but
 243 do not include D-O events. Across the remaining 60 sites, we identified 278 out of the 348
 244 individual D-O events (80%) that occurred during the intervals covered by the records. In the
 245 majority of cases where a D-O event should have been registered but could not be identified in
 246 an individual record (60 out of 70 cases), the resolution of that part of the record was extremely
 247 poor (≤ 3 samples in the 900-year interval starting 300 years before to 600 years after the
 248 official start date of the event).

249 Changes in both MTCO and MTWA were generally largest in the extratropics and were more
 250 muted in the tropics (Figure 3). The change in MTCO was significantly larger in the northern

251 ~~extratropics when considered across all D-O events and sites; the change in MTCO was larger,~~
252 ~~but not significantly larger, in the southern extratropics; the changes in MTCO are not~~
253 ~~correlated with the changes in MTWA in the tropics (Table 3). There is a significant positive~~
254 ~~relationship between the change in α and the change in MTWA in all regions (Figure 4; Table~~
255 ~~4).~~

256 ~~The use of dynamic time warping made it possible to identify D-O events robustly (Table 1).~~
257 ~~Across the 73 sites, we identified 204 out of the 210 individual D-O events that occurred during~~
258 ~~the intervals covered by the records. In the majority of cases where a D-O event should have~~
259 ~~been registered but could not be identified in an individual record (5 out of 6 cases), the~~
260 ~~resolution of that part of the record was extremely poor (≤ 3 samples in the 900-year interval~~
261 ~~starting 300 years before to 600 years after the official start date of the event).~~

262 ~~Changes in both MTCO and MTWA were generally largest in the extratropics and were more~~
263 ~~muted in the tropics (Figure 3). The change in MTCO was larger, but not significantly larger,~~
264 ~~in the northern extratropics when considered across all D-O events and sites; the change in~~
265 ~~MTCO was smaller, but not significantly smaller, in the southern extratropics; the changes in~~
266 ~~MTCO are not correlated with the changes in MTWA in the tropics (Table 3). There is a~~
267 ~~significant positive relationship between the change in α and the change in MTWA in all~~
268 ~~regions (Figure 4; Table 4).~~

269 The spatial patterns of changes in MTCO and MTWA show consistent features across multiple
270 D-O events (Figure 5), most noticeably that the largest warming occurs in the extratropics of
271 ~~Europe and Eurasia~~Eurasia, while western North America and the southern extratropics are
272 characterised by cooling. The anti-phasing between the northern and southern extratropics is
273 consistent across D-O events. Nevertheless, both the magnitude of the changes and the spatial
274 patterns vary between the D-O events (~~Figure S2~~Figure S3; ~~Figure S3~~Figure S4). Changes in
275 α broadly follow the changes in temperature, with increased α in regions characterised by
276 warming (Figure 5) but show more variability both spatially and between D-O events (~~Figure~~
277 ~~S4~~Figure S5). This is particularly true for Europe, which is characterised by a mixed signal of
278 drying and wetting.

279 4. Discussion and Conclusions

280 We have presented a first attempt to map the spatial patterns of quantitative changes in seasonal
281 temperature and plant-available moisture during D-O events globally, using a consistent
282 methodology and a single data source. These analyses show that there is an anti-phasing
283 between changes in the northern extratropics and the southern extratropics, with warming in
284 the north and cooling in the south. The largest and most consistent warming during D-O events
285 occurs in ~~Europe and Eurasia~~Eurasia. There is a significant difference in the warming during
286 winter and summer in the northern extratropics, resulting in an overall reduction in seasonality,
287 but no significant difference in the tropics and southern extratropics. Site-based reconstructions
288 (e.g. Denton et al., 2022; Zander et al., 2024) suggest much larger cooling in winter than
289 summer during cold phases of the last glacial, implying enhanced seasonality compared to
290 warm intervals, which would be consistent with our reconstructions of a reduction in
291 seasonality during warming events in the northern extratropics. ~~There is no indication of a~~
292 ~~significant difference in the temperature change during winter and summer, and thus no~~
293 ~~indication of a large shift in seasonality as inferred from some site-based reconstructions (e.g.~~
294 ~~Zander et al., 2023).~~ Globally, there is a positive relationship between the change in
295 temperature and plant available moisture, as indicated by α . This is consistent with more
296 qualitative interpretation of palaeo-records from specific regions, where many regions are
297 characterised by both warming and wetting (e.g. western Europe: Sánchez Goñi et al., 2008;
298 Fletcher et al., 2010; eastern Europe: Fleitmann et al., 2009; Stockehecke et al., 2016; central
299 Siberia: Grygar et al., 2006; the Great Basin USA: Denniston et al., 2007; Jiménez-Moreno et
300 al., 2010). However, according to our reconstructions, the nature of this relationship varies
301 between regions: there are some regions that are characterised by warming and wetting, others
302 are characterised by warming and drying. Previous studies have also indicated drier conditions
303 during D-O events, particularly in parts of the USA such as the Pacific Northwest (Grigg and
304 Whitlock, 2002) and Florida (Grimm et al., 2006; Jiménez-Moreno et al., 2010) Although there
305 is some consistency in the broadscale patterns of changes across D-O events, the magnitude of
306 the changes as well as the spatial patterning varies between events.

307 We have used a global pollen data set for calibration of the pollen-climate relationships,
308 SMPDsv2 (Villegas-Diaz and Harrison, 2022). The use of a global data set, rather than region-
309 specific training data, relies on the principle of phylogenetic niche conservatism (Harvey and
310 Pagel, 1991), which states that traits tend to remain constant over time. This also applies to the

311 climate niche (Wiens and Graham, 2005; Wiens et al., 2010; Peterson, 2011; Crisp and Cook,
312 2012; Jiang et al., 2023) as evidenced by disjunct distributions of taxa across different
313 continents (Yin et al., 2021). Niche conservatism underpins the fact that the modern
314 distribution of specific genera can be predicted using climate-pollen relationships developed
315 from other regions (e.g. Huntley et al., 1989). The use of a global data set for calibration makes
316 it possible to sample a large range of climates, and thus makes it more likely that the
317 reconstructions of glacial climates are realistic and not confined to the limited climate range
318 sampled in any one region (Turner et al., 2020). Indeed, Turner et al. (2020) have shown that
319 increasing the size of the calibration data set tends to lead to smaller reconstruction errors and
320 more accurate estimates of taxon coefficients. Pragmatically, the use of a global data set also
321 facilitates making reconstructions for sites from regions where there is limited modern pollen
322 data.

323 These reconstructions can be used as targets for model evaluation, specifically the two transient
324 D-O experiments planned for the next phase of the Palaeoclimate Modelling Intercomparison
325 (see Malmierca-Vallet et al., 2023 for the experimental protocol). The first of these experiments
326 is a baseline simulation starting at 34 ka, a time with low obliquity, moderate MIS3 greenhouse
327 gas values, and an intermediate ice sheet configuration, which appears to be most conducive to
328 generating D–O-like behaviour in climate models. The second experiment involves the
329 addition of freshwater, to examine whether ~~this is necessary~~ this is necessary to precondition a
330 state conducive to generating D–O events. The observed anti-phasing in temperature changes
331 between the northern and southern hemispheres is a general feature of climate model
332 experiments. Most models show larger warming in winter than in summer in the northern
333 hemisphere (e.g. Flückiger et al., 2008; Van Meersbeeck et al., 2011; Izumi et al., 2023), which
334 is also consistent with our reconstructions. However, most models show larger warming in
335 winter than in summer in the northern hemisphere (e.g. Flückiger et al., 2008; Van Meersbeeck
336 et al., 2011; Izumi et al., 2023), which is not consistent with our reconstructions. Models
337 generally show an intensification of the northern hemisphere monsoons during D-O events
338 (e.g. Menviel et al., 2020; Izumi et al., 2023), but there is less consistency about changes in
339 plant-available moisture in the extratropics. Our reconstructions of α suggest an intensification
340 of the northern hemisphere monsoons, consistent with the simulations, and provide an
341 opportunity to evaluate spatial patterns of moisture changes over the extratropics. Models
342 generally show an intensification of the northern hemisphere monsoons during D-O events
343 (e.g. Menviel et al., 2020; Izumi et al., 2023), but there is less consistency about changes in

~~plant-available moisture in the extratropics. The reconstructions also indicate an increase in α across much of the tropics, including northern South America, West Africa and southern China and Japan. Although α is not a direct reflection of summer precipitation, these changes are consistent with enhanced northern hemisphere monsoons during warming events, as shown by speleothem records from the Caribbean (Warken et al, 2019) and speleothem and pollen records from Asia (Wang et al., 2001; Zorzi et al., 2022; Fohlmeister et al., 2023). Although there is some consistency in the broadscale patterns of changes in temperature and moisture across D-O events, the magnitude of the changes as well as the spatial patterning varies between events.~~

~~Our reconstructions of α suggest an intensification of the monsoon over northern South America but there are no records from other northern hemisphere monsoon regions. However, the records do provide an opportunity to evaluate moisture changes over the extratropics.~~

~~Identifying D-O events in pollen records is often problematic, particularly in regions where warming (especially if accompanied by dryer conditions) leads to a reduction (or an hiatus) in sedimentation as reflected in the variable resolution of the available pollen records (e.g. Sinopoli et al., 2019; Wei et al., 2021; Camuera et al., 2022; Pini et al., 2022). The use of shorter periods (Alshehri et al., 2019) goes some way to improving the identification of potential D-O events using dynamic time warping (Alshehri et al., 2019). Nevertheless, we were able to identify D-O events only 80% of the 348 individual D-O events that occurred during the intervals covered by the 60 records available globally. It is also likely that some of the variability in the reconstructed changes between different D-O events reflects imperfect identification of specific events because of the comparatively modest resolution of the records. Several new high-resolution records covering MIS3 have become available since the compilation of the ACER database (e.g. Bird et al., 2024; Wei et al., 2021; Camuera et al., 2022; Pini et al., 2022; Rowe et al., 2024; Shichi et al., 2023; Zorzi et al., 2022) and including these newer records could help to improve the reliability of the global reconstructions presented here. Nevertheless, this first compilation of quantitative climate reconstructions through multiple D-O events during MIS3 provides an opportunity for evaluation of the transient D-O simulations planned as part of the next phase of the Palaeoclimate Modelling Intercomparison Project (Malmierca-Vallet et al., 2023).~~

~~Identifying D-O events in pollen records is often problematic, particularly in regions where warming (especially if accompanied by dryer conditions) leads to a reduction (or an hiatus) in sedimentation as reflected in the variable resolution of the available pollen records (e.g.~~

~~Sinopoli et al., 2019; Wei et al., 2021; Camuera et al., 2022; Pini et al., 2022). Interpolation of the reconstructed climate between more sparsely spaced samples goes some way to improving the identification of potential D-O events using dynamic time warping, as does the use of shorter periods (Alshehri et al., 2019). However, it is likely that some of the variability in the reconstructed changes between different D-O events reflects imperfect identification of specific events because of the comparatively modest resolution of the records. Several new high-resolution records covering MIS3 have become available since the compilation of the ACER database (e.g. Wei et al., 2021; Camuera et al., 2022; Pini et al., 2022) and including these newer records could help to improve the reliability of the global reconstructions presented here. Nevertheless, this first compilation of quantitative climate reconstructions through multiple D-O events during MIS3 provides an opportunity for evaluation of the transient D-O simulations planned as part of the next phase of the Palaeoclimate Modelling Intercomparison Project (Malmierca Vallet et al., 2023).~~

Data and code availability. All the data used are public access and cited here. The code used to generate the reconstructions and figures is available at <https://github.com/ml4418/DO-climate-reconstruction-paper.git>

Author contributions. ML, SPH and ICP designed the study. ML made the reconstructions and produced the figures and tables. ML and SPH carried out the analyses. SPH wrote the first draft of the paper and all authors contributed to the final draft.

Competing Interests. The authors declare not competing interests.

Acknowledgements. ML acknowledges support from Imperial College through the Lee Family Scholarship. ICP acknowledges support from the ERC under the European Union Horizon 2020 research and innovation programme (grant agreement no.: 787203 REALM). SPH acknowledges fruitful discussions with colleagues from the D-O community working group.

References

- 404 Adolphi, F., Bronk Ramsey, C., Erhardt, T., Edwards, R. L., Cheng, H., Turney, C. S. M.,
405 Cooper, A., Svensson, A., Rasmussen, S. O., Fischer, H., and Muscheler, R.:
406 Connecting the Greenland ice-core and U / Th timescales via cosmogenic
407 radionuclides: testing the synchronicity of Dansgaard–Oeschger events, *Clim. Past*, 14,
408 1755–1781, <https://doi.org/10.5194/cp-14-1755-2018>, 2018.
- 409 Alshehri, M., Coenen, F., and Dures, K.: Effective sub-sequence-based dynamic time warping.
410 In: Bramer, M., Petridis, M. (eds) *Artificial Intelligence XXXVI. SGAI 2019. Lecture*
411 *Notes in Computer Science*, 11927. Springer, Cham. [https://doi.org/10.1007/978-3-](https://doi.org/10.1007/978-3-030-34885-4_23)
412 [030-34885-4_23](https://doi.org/10.1007/978-3-030-34885-4_23), 2019.
- 413 Ampel, L., Bigler, C., Wohlfarth, B., Risberg, J., Lotter, A.F., and Veres, D.: Modest summer
414 temperature variability during DO cycles in western Europe, *Quat. Sci. Rev.*, 29, 1322–
415 1327, <https://doi.org/10.1016/j.quascirev.2010.03.002>, 2010.
- 416 Bauska, T. K., Marcott, S. A. and Brook, E. J.: Abrupt changes in the global carbon cycle
417 during the last glacial period, *Nat. Geosci.*, 14(2), 91–96, doi:10.1038/s41561-020-
418 00680-2, 2021.
- 419 Bellman, R., and Kalaba, R.: On adaptive control processes, *Automatic Control*, IRE
420 *Transactions*, 4, 1–9, http://ieeexplore.ieee.org/xpls/abs_all.jsp?arnumber=1104847,
421 1959.
- 422 [Bird, M., Brand, M., Comley, R., Fu, X., Hadeen, X., Jacobs, Z., Rowe, C., Wurster, C., Zwart,](#)
423 [C. and Bradshaw, C.: Late Pleistocene emergence of an anthropogenic fire regime in](#)
424 [Australia’s tropical savannahs, *Nat. Geosci.*, 17, doi:10.1038/s41561-024-01388-3,](#)
425 [2024.](#)
- 426
- 427 Burstyn, Y., Gazit, A., and Omri Dvir, O.: Hierarchical Dynamic Time Warping methodology
428 for aggregating multiple geological time series, *Comp. & Geosci.*, 150, 104704,
429 <https://doi.org/10.1016/j.cageo.2021.104704>, 2021.
- 430 Camuera, J., Ramos-Román, M.J., Jiménez-Moreno, G. *et al.*: Past 200 kyr hydroclimate
431 variability in the western Mediterranean and its connection to the African Humid
432 Periods, *Sci. Rep.*, 12, 9050, <https://doi.org/10.1038/s41598-022-12047-1>, 2022.

433 Corrick, E.C., Drysdale, R.N., Hellstrom, J.C., Capron, E., Rasmussen, S.O., Zhang, X.,
434 Fleitmann, D., Couchoud, I., and Wolff, E.: Synchronous timing of abrupt climate
435 changes during the last glacial period, *Science*, 369, 963–969,
436 <https://doi.org/10.1126/science.aay5538>, 2020.

437 [Crisp, M. D. and Cook, L. G.: Phylogenetic niche conservatism: What are the underlying](#)
438 [evolutionary and ecological causes?, *New Phytol.*, 196\(3\), 681–694,](#)
439 [doi:10.1111/j.1469-8137.2012.04298.x, 2012.](#)

440

441 Dansgaard, W., Johnsen, S.J., Clausen, H.B., Dahl-Jensen, D., Gundestrup, N.S., Hammer,
442 C.U., Hvidberg, C.S., Steffensen, J.P., Sveinbjörnsdottir, A.E., Jouzel, J., and Bond,
443 G.: Evidence for general instability of past climate from a 250-kyr ice-core record,
444 *Nature*, 364, 218–220, <https://doi.org/10.1038/364218a0>, 1993.

445 Denniston, R.F., Asmerom, Y., Polyak, V., Dorale, J.A., Carpenter, S.J., Trodick, C., Hoyer,
446 B., and González, L.A.: Synchronous millennial-scale climatic changes in the Great
447 Basin and the North Atlantic during the last interglacial. *Geology* 35, 619–622, 2007.

448 [Doblas-Reyes, F. J., Sörensson, A. A., Almazroui, M., Dosio, A., Gutowski, W. J., Haarsma,](#)
449 [R., Hamdi, R., Hewitson, B., Kwon, W.-T., Lamptey, B. L., Maraun, D., Stephenson,](#)
450 [T. S., Takayabu, I., Terray, L., Turner, A. and Zuo, Z.: Linking global to regional](#)
451 [climate change, in *Climate Change 2021 – The Physical Science Basis: Working Group*](#)
452 [I Contribution to the Sixth Assessment Report of the Intergovernmental Panel on](#)
453 [Climate Change, edited by V. Masson-Delmotte, P.Zhai, A. Pirani, S. L. Connors, C.](#)
454 [Péan, S. Berger, N. Caud, Y. Chen, L. Goldfarb, M. I. Gomis, M. Huang, K. Leitzell,](#)
455 [E.Lonnoy, J. B. R. Matthews, T. K. Maycock, T. Waterfield, O. Yelekçi, R. Yu, and B.](#)
456 [Zhou, pp. 1363–1512, Cambridge University Press, Cambridge, United Kingdom and](#)
457 [New York, NY, USA., 2021.](#)

458 Fleitmann, D., Cheng, H., Badertscher, S., Edwards, R.L., Mudelsee, M., Göktürk, O.M.,
459 Fankhauser, A., Pickering, R., Raible, C.C., Matter, A., Kramers, J., and Tüysüz, O.:
460 Timing and climatic impact of Greenland interstadials recorded in stalagmites from
461 northern Turkey, *Geophys. Res. Lett.*, 36, 2009.

- 462 Fletcher, W.F., Sánchez Goñi, M.F., Allen, J.R.M., Cheddadi, R., Combourieu-Nebout, N.,
463 Huntley, B., Lawson, I., Londeix, L., Magri, D., Margari, V., Müller, U.C., Naughton,
464 F., Novenko, E., Roucoux, K., Tzedakis, P.C.: Millennial-scale variability during the
465 last glacial in vegetation records from Europe, *Quat. Sci. Rev.*, 29, 2839-2864,
466 <https://doi.org/10.1016/j.quascirev.2009.11.015>, 2010.
- 467 Flückiger, J., Knutti, R., White, J.W.C., and Renssen, H.: Modeled seasonality of glacial abrupt
468 climate events, *Clim. Dyn.*, 31, 633–645, <https://doi.org/10.1007/s00382-008-0373-y>,
469 2008.
- 470 [Fohlmeister, J., Sekhon, N., Columbu, A., Vettoretti, G., Weitzel, N., Rehfeld, K., Veiga-Pires,](#)
471 [C., Ben-Yami, M., Marwan, N. and Boers, N.: Global reorganization of atmospheric](#)
472 [circulation during Dansgaard–Oeschger cycles, *Proc. Natl. Acad. Sci.*, 120\(36\),](#)
473 [e2302283120, doi:10.1073/pnas.2302283120, 2023.](#)
- 474
- 475 Grigg, L.D., and Whitlock, C.: Patterns and causes of millennial-scale climate change in the
476 Pacific Northwest during Marine Isotope Stages 2 and 3, *Quat. Sci. Rev.*, 21, 2067-
477 2083, 2002.
- 478 Grimm, E.C., Watts, W.A., Jacobson, G.L., Hansen, B.C.S., Almquist, H., and Dieffenbacher-
479 Krall, A.C.: Evidence for warm wet Heinrich events in Florida, *Quat. Sci. Rev.*, 25,
480 2197-2211, 2006.
- 481 Grygar, T., Kadlec, J., Pruner, P., Swann, G., Bezdicka, P., Hradil, D., Lang, K., Novotna, K.,
482 and Oberhänsli, H.: Paleoenvironmental record in Lake Baikal sediments:
483 environmental changes in the last 160 ky, *Palaeogeogr. Palaeoclimatol. Palaeoecol.*,
484 237, 240-254, 2006.
- 485 Guiot, J., de Beaulieu, J. L., Cheddadi, R., David, F., Ponel, P., and Reille, M.: The climate in
486 Western Europe during the last Glacial/Interglacial cycle derived from pollen and insect
487 remains, *Palaeogeogr., Palaeoclimatol., Palaeoecol.*, 103, 73–93,
488 [https://doi.org/10.1016/0031-0182\(93\)90053-L](https://doi.org/10.1016/0031-0182(93)90053-L), 1993.
- 489 Jiménez-Moreno, G., Anderson, R.S., Desprat, S., Grigg, L.D., Grimm, E.C., Heusser, L.E.,
490 Jacobs, B.F., López-Martínez, C., Whitlock, C.L., and Willard, D.A.: Millennial-scale

491 variability during the last glacial in vegetation records from North America, *Quat. Sci.*
492 *Rev.*, 29, 2865-2881, <https://doi.org/10.1016/j.quascirev.2009.12.013>, 2010.

493 Harrison, S.P., and Sánchez Goñi, M.F.: Global patterns of vegetation response to millennial-
494 scale variability during the last glacial: A synthesis. *Quat. Sci. Rev.*, 29, 2957-2980,
495 2010.

496 [Harvey, P. H. and Pagel, M. D.: The comparative method in evolutionary biology, Oxford](#)
497 [University Press., 1991.](#)

498

499 Huber, C., Leuenberger, M., Spahni, R., Flückiger, J., Schwander, J., Stocker, T.F., Johnsen,
500 S., Landais, A., and Jouzel, J.: Isotope calibrated Greenland temperature record over
501 Marine Iso- tope Stage 3 and its relation to CH₄, *Earth Planet. Sci. Lett.*, 243, 504–519,
502 2006.

503 [Huntley, B., Bartlein, P. J. and Prentice, I. C.: Climatic control of the distribution and](#)
504 [abundance of Beech \(Fagus L.\) in Europe and North America, *J. Biogeogr.*, 16\(6\), 551–](#)
505 [560, doi:10.2307/2845210, 1989.](#)

506

507 Huntley, B., Watts, W.A., Allen, J.R.M., Zolitschka, B.: Palaeoclimate, chronology and
508 vegetation history of the Weichselian Lateglacial: comparative analysis of data from
509 three cores at Lago Grande di Monticchio, southern Italy, *Quat. Sci. Rev.*, 18: 945-960,
510 [https://doi.org/10.1016/S0277-3791\(99\)00007-4](https://doi.org/10.1016/S0277-3791(99)00007-4), 1999.

511 [IPCC: Climate change 2022: Impacts, adaptation and vulnerability. Contribution of working](#)
512 [group II to the sixth assessment report of the Intergovernmental Panel on Climate](#)
513 [Change, edited by H.-O. Pörtner, D. C. Roberts, M. Tignor, E. S. Poloczanska, K.](#)
514 [Mintenbeck, A. Alegría, M. Craig, S. Langsdorf, S. Löschke, V. Möller, A. Okem, and](#)
515 [B. Rama, Cambridge University Press, Cambridge University Press, Cambridge, UK](#)
516 [and New York, NY, USA., 2022.](#)

- 517 [Jiang, K., Wang, Q., Dimitrov, D., Luo, A., Xu, X., Su, X., Liu, Y., Li, Y., Li, Y. and Wang, Z.:](#)
518 [Evolutionary history and global angiosperm species richness–climate relationships,](#)
519 [Glob. Ecol. Biogeogr., 32\(7\), 1059–1072, doi:10.1111/geb.13687, 2023.](#)
- 520
- 521 Kindler, P., Guillevic, M., Baumgartner, M., Schwander, J., Landais, A., and Leuenberger, M.:
522 Temperature reconstruction from 10 to 120 kyr b2k from the NGRIP ice core, *Clim.*
523 *Past*, 10, 887–902, <https://doi.org/10.5194/cp-10-887-2014>, 2014.
- 524 [Lee, J.-Y., Marotzke, J., Bala, G., Cao, L., Corti, S., Dunne, J. P., Engelbrecht, F., Fischer, E.,](#)
525 [Eyfe, J. C., Jones, C., Maycock, A., Mutemi, J., Ndiaye, O., Panickal, S. and Zhou, T.:](#)
526 [Future global climate: Scenario-based projections and near-term information, in](#)
527 [Climate change 2021: The physical science basis. Contribution of working group I to](#)
528 [the sixth assessment report of the Intergovernmental Panel on Climate Change, edited](#)
529 [by V. Masson-Delmotte, P. Zhai, A. Pirani, S. L. Connors, C. Péan, S. Berger, N. Caud,](#)
530 [Y. Chen, L. Goldfarb, M. I. Gomis, M. Huang, K. Leitzell, E. Lonnoy, J. B. R.](#)
531 [Matthews, T. K. Maycock, T. Waterfield, O. Yelekçi, R. Yu, and B. Zhou, pp. 553–672,](#)
532 [Cambridge University Press, Cambridge, United Kingdom and New York, NY, USA.,](#)
533 [2021.](#)
- 534
- 535 Liu, M., Prentice, I.C., ter Braak, C.J.F, and Harrison, S.P.: An improved statistical approach
536 for reconstructing past climates from biotic assemblages, *Proc. Royal Soc., Math. A,*
537 *476*, 20200346, 20200346, <https://doi.org/10.1098/rspa.2020.0346>, 2020.
- 538 Liu, M., Shen, Y., González-Sampériz, P., Gil-Romera, G., ter Braak, C.J.F. Prentice, I.C., and
539 Harrison, S.P.: Holocene climates of the Iberian Peninsula, *Clim. Past* 19, 803-834,
540 <https://doi.org/10.5194/cp-19-803-2023>, 2023.
- 541 Malmierca-Vallet, I., Sime, L.C., and the D–O community members: Dansgaard–Oeschger
542 events in climate models: review and baseline Marine Isotope Stage 3 (MIS3) protocol,
543 *Clim. Past*, 19, 915–942, <https://doi.org/10.5194/cp-19-915-2023>, 2023.

- 544 Menviel, L., Timmermann, A., Friedrich, T., and England, M. H.: Hindcasting the continuum
545 of Dansgaard–Oeschger variability: mechanisms, patterns and timing, *Clim. Past* 10,
546 63–77, 2014.
- 547 Menviel, L.C., Skinner, L.C., Tarasov, L., and Tzedakis, P.C.: An ice–climate oscillatory
548 framework for Dansgaard–Oeschger cycles, *Nat. Rev. Earth Environ.*, 1, 677–693,
549 <https://doi.org/10.1038/s43017-020-00106-y>, 2020.
- 550 [Peterson, A. T.: Ecological niche conservatism: A time-structured review of evidence, *J.*](#)
551 [*Biogeogr.*, 38\(5\), 817–827, doi:10.1111/j.1365-2699.2010.02456.x, 2011.](#)
- 552
- 553 Pini, R., Furlanetto, G., Vallé, F., Badino, F., Wick, L., Anselmetti, F.S., Bertuletti, P., Fusi, N.,
554 Morlock, M.A., Delmonte, B., Harrison, S.P., Maggi, V., Ravazzi, C.: Linking North
555 Atlantic and Alpine Last Glacial Maximum climates via a high-resolution pollen-based
556 subarctic forest steppe record, *Quat. Sci. Rev.*, 294, 107759,
557 <https://doi.org/10.1016/j.quascirev.2022.107759>, 2022.
- 558 Prentice, I. C., Villegas-Diaz, R. and Harrison, S. P.: Accounting for atmospheric carbon
559 dioxide variations in pollen-based reconstruction of past hydroclimates, *Glob. Planet.*
560 *Change*, 211, 103790, doi:10.1016/j.gloplacha.2022.103790, 2022.
- 561 Prud'homme, C., Fischer, P., Jöris, O., Gromov, S., Vinnepand, M., Hatté, C., Vonhof, H.,
562 Moine, O., Vött, A., and Fitzsimmons, K. E.: Millennial-timescale quantitative
563 estimates of climate dynamics in central Europe from earthworm calcite granules in
564 loess deposits, *Commun. Earth Environ.*, 3, 1–14, [https://doi.org/10.1038/s43247-022-](https://doi.org/10.1038/s43247-022-00595-3)
565 [00595-3](https://doi.org/10.1038/s43247-022-00595-3), 2022.
- 566 [Rowe, C., Brand, M., Wurster, C. M. and Bird, M. I.: Vegetation changes through stadial and](#)
567 [interstadial stages of MIS 4 and MIS 3 based on a palynological analysis of the](#)
568 [Girraween Lagoon sediments of Darwin, Australia, *Palaeogeogr. Palaeoclimatol.*](#)
569 [*Palaeoecol.*, 642, 112150, doi:10.1016/j.palaeo.2024.112150, 2024.](#)
- 570 [Sánchez Goñi, M., Cacho, I., Turon, J., Guiot, J., Sierro, F., Peyrouquet, J., Grimalt, J. and](#)
571 [Shackleton, N.: Synchronicity between marine and terrestrial responses to millennial](#)

572 [scale climatic variability during the last glacial period in the Mediterranean region,](#)
 573 [Clim. Dyn., 19\(1\), 95–105, doi:10.1007/s00382-001-0212-x, 2002.](#)

574

575 Sánchez Goñi, M.F., and Harrison, S.P.: Millennial-scale climate variability and vegetation
 576 changes during the Last Glacial: Concepts and terminology, *Quat. Sci. Rev.*, 29, 2823–
 577 2827, 2010.

578 Sánchez Goñi, M.F., Desprat, S., Danialu, A.-L., Bassinot, F., Polanco-Martínez, J.M., Harrison,
 579 S.P., Allen, J.R.P., Anderson, R.S., Behling, H., Bonnefille, R., Burjachs, F., Carrión,
 580 J.S., Cheddadi, R., Clark, J.S., Combourieu-Nebout, N., Courtney-Mustaphi, C.,
 581 Debusk, G.H., Dupont, L.M., Finch, J., Fletcher, W.J., Giardini, M., González, C.,
 582 Gosling, W.D., Grigg, L.D., Grimm, E.C., Hayashi, R., Helmens, K., Heusser, L.E.,
 583 Hill, T., Hope, G., Huntley, B., Igarashi, Y., Irino, T., Jacobs, B.F., Jiménez-Moreno, G.,
 584 Kawai, S., Kershaw, P., Kumon, F., Lawson, I., Ledru, M.-P., Lézine, A.-M., Liew, P.-
 585 M., Magri, D., Marchant, R., Margari, V., Mayle, F., McKenzie, M., Moss, P., Müller,
 586 S., Müller, U.C., Naughton, F., Newnham, R.M., Oba, T., Pérez-Obiol, R., Pini, R.,
 587 Ravazzi, C., Roucoux, K.H., Rucina, S., Scott, L., Takahara, H., Tzedakis, P.C., Urrego,
 588 D.H., Van Geel, B., Valencia, B.G., Vandergoes, M.J., Vincens, A., Whitlock, C.L.,
 589 Willard, D. A., and Yamamoto, M.: The ACER pollen and charcoal database: a global
 590 resource to document vegetation and fire response to abrupt climate changes of the last
 591 glacial period, *Earth Syst. Sci. Data* 9: 679-695, 2017.

592 [Shichi, K., Goebel, T., Izuho, M. and Kashiwaya, K.: Climate amelioration, abrupt vegetation](#)
 593 [recovery, and the dispersal of Homo sapiens in Baikal Siberia, *Sci. Adv.*, 9\(38\),](#)
 594 [eadi0189, doi:10.1126/sciadv.adi0189, 2024.](#)

595

596 Sinopoli, G., Peyron, O., Masi, A., Holtvoeth, J., Francke, A., Wagner, B., and Sadori, L.:
 597 Pollen-based temperature and precipitation changes in the Ohrid Basin (western
 598 Balkans) between 160 and 70 ka, *Clim. Past*, 15, 53–71, [https://doi.org/10.5194/cp-15-](https://doi.org/10.5194/cp-15-53-2019)
 599 [53-2019](https://doi.org/10.5194/cp-15-53-2019), 2019.

600 Stockhecke, M., Timmermann, A., Kipfer, R., Haug, G.H., Kwiecien, O., Friedrich, T.,
601 Menviel, L., Litt, T., Pickarski, N., and Anselmetti, F.S.: Millennial to orbital-scale
602 variations of drought intensity in the Eastern Mediterranean, *Quat. Sci. Rev.*, 133, 77-
603 95, 2016.

604 [Turner, M. G., Wei, D., Prentice, I. C. and Harrison, S. P.: The impact of methodological](#)
605 [decisions on climate reconstructions using WA-PLS, *Quat. Res.*, 99, 341–356,](#)
606 [doi:10.1017/qua.2020.44, 2021.](#)

607

608 Újvári, G., Bernasconi, S. M., Stevens, T., Kele, S., Páll-Gergely, B., Surányi, G., and Demény,
609 A.: Stadial-Interstadial Temperature and Aridity Variations in East Central Europe
610 Preceding the Last Glacial Maximum, *Paleoceanog. Paleoclim.*, 36, e2020PA004170,
611 <https://doi.org/10.1029/2020PA004170>, 2021.

612 Van Meerbeeck, C.J., Renssen, H., Roche, D.M., Wohlfarth, B., Bohncke, S.J.P., Bos, J.A.A.,
613 Engels, S., Helmens, K.F., Sánchez-Goñi, M.F., Svensson, A., and Vandenberghe, J.:
614 The nature of MIS 3 stadial-interstadial transitions in Europe: New insights from
615 model-data comparisons, *Quat. Sci. Rev.*, 30, 3618–3637,
616 <https://doi.org/10.1016/j.quascirev.2011.08.002>, 2011.

617 Villegas-Diaz, R., and Harrison, S.P.: The SPECIAL Modern Pollen Data Set for Climate
618 Reconstructions, version 2 (SMPDSv2). University of Reading.
619 Dataset. <https://doi.org/10.17864/1947.000389>, 2022.

620 Voelker, A.H.: Global distribution of centennial-scale records for Marine Isotope Stage (MIS)
621 3: a database, *Quat. Sci. Rev.*, 21, 1185–1212, 2002.

622 [Wang, Y. J., Cheng, H., Edwards, R. L., An, Z. S., Wu, J. Y., Shen, C.-C. and Dorale, J. A.: A](#)
623 [high-resolution absolute-dated Late Pleistocene monsoon record from Hulu Cave,](#)
624 [China, *Science \(80-. \)*, 294\(5550\), 2345–2348, doi:10.1126/science.1064618, 2001.](#)

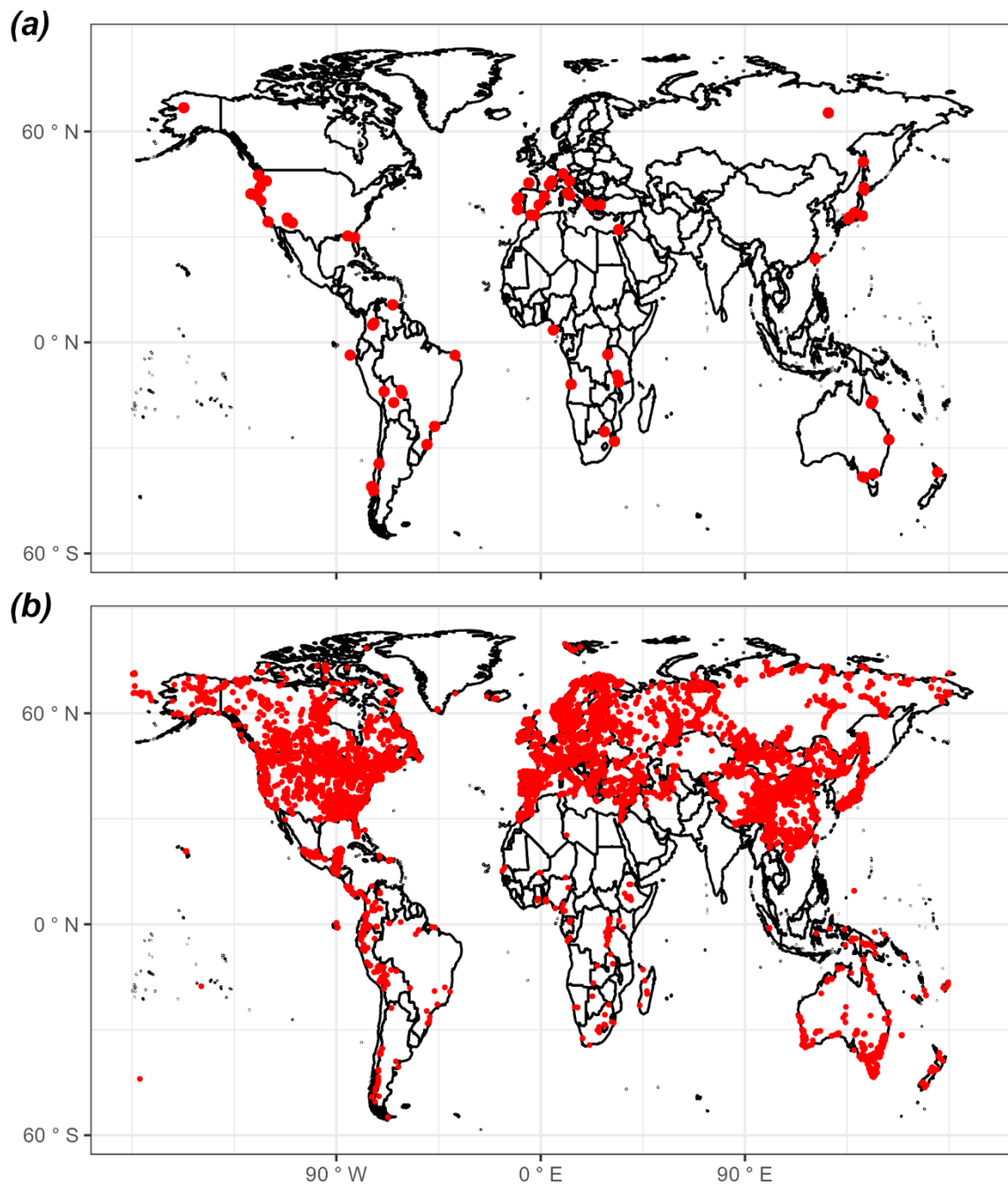
625

- 626 [Warken, S. F., Scholz, D., Spötl, C., Jochum, K. P., Pajón, J. M., Bahr, A. and Mangini, A.:](#)
627 [Caribbean hydroclimate and vegetation history across the last glacial period, *Quat. Sci.*](#)
628 [Rev., 218, 75–90, doi:10.1016/j.quascirev.2019.06.019, 2019.](#)
- 629 Wei, D., González-Sampériz, P., Gil-Romera, G., Harrison, S.P., and Prentice, I.C.: Seasonal
630 temperature and moisture changes in interior semi-arid Spain from the last interglacial
631 to the Late Holocene, *Quat. Res.*, 101, 143–155, <https://doi.org/10.1017/qua.2020.108>,
632 2021.
- 633 [Wiens, J. and Graham, C.: Niche conservatism: Integrating evolution, ecology, and](#)
634 [conservation biology, *Annu. Rev. Ecol. Evol. Syst.*, 36, 519–539,](#)
635 [doi:10.1146/annurev.ecolsys.36.102803.095431, 2005.](#)
- 636 Wolff, E. W., Chappellaz, J., Blunier, T., Rasmussen, S. O. and Svensson, A.: Millennial-scale
637 variability during the last glacial: The ice core record, *Quat. Sci. Rev.*, 29(21), 2828–
638 2838, doi:10.1016/j.quascirev.2009.10.013, 2010.
- 639 [Yin, X., Jarvie, S., Guo, W.-Y., Deng, T., Mao, L., Zhang, M., Chu, C., Qian, H., Svenning, J.-](#)
640 [C. and He, F.: Niche overlap and divergence times support niche conservatism in](#)
641 [eastern Asia–eastern North America disjunct plants, *Glob. Ecol. Biogeogr.*, 30\(10\),](#)
642 [1990–2003, doi:10.1111/geb.13360, 2021.](#)
- 643
- 644 [Zander, P. D., Böhl, D., Sirocko, F., Auderset, A., Haug, G. H. and Martínez-García, A.:](#)
645 [Reconstruction of warm-season temperatures in central Europe during the past 60 000](#)
646 [years from lacustrine branched glycerol dialkyl glycerol tetraethers \(brGDGTs\), *Clim.*](#)
647 [Past, 20\(4\), 841–864, doi:10.5194/cp-20-841-2024, 2024.](#)
- 648 [Zorzi, C., Desprat, S., Clément, C., Thirumalai, K., Oliviera, D., Anupama, K., Prasad, S. and](#)
649 [Martinez, P.: When eastern India oscillated between desert versus savannah-dominated](#)
650 [vegetation, *Geophys. Res. Lett.*, 49\(16\), e2022GL099417,](#)
651 [doi:10.1029/2022GL099417, 2022.](#)~~Zander, P.D., Böhl, D., Sirocko, F., Auderset, A.,~~
652 ~~Haug, G., and Martínez-García, A.: Reconstruction of warm season temperatures in~~
653 ~~central Europe during the past 60,000 years from lacustrine GDGTs, *EGUsphere*~~
654 ~~[preprint], <https://doi.org/10.5194/egusphere-2023-1960>, 2023.~~

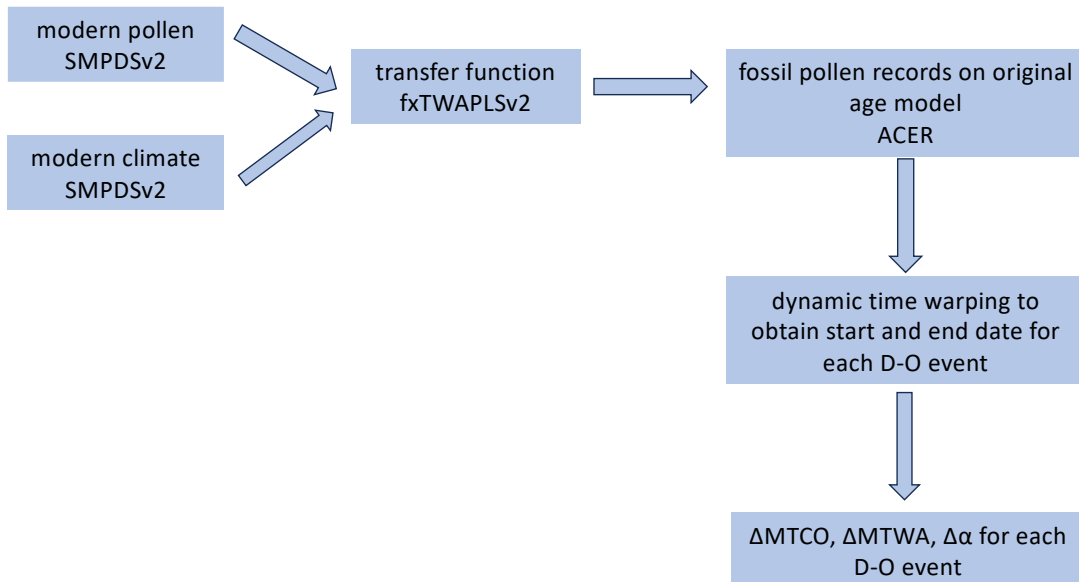
655
|
656

657 **Figures and Tables**

658 Figure 1: Map showing the locations of sites (a) from the Abrupt Climate Changes and
659 Environmental Responses (ACER) database (Sánchez Goñi et al., 2017) covering the interval
660 between 50 ka and 30 ka used for the reconstructions and (b) sites in version 2 of the SPECIAL
661 Modern Pollen Data Set (SMPDSv2: Villegas-Diaz and Harrison, 2022) used to derive the
662 transfer functions for these climate reconstructions.



665 Figure 2: Flow chart showing the reconstruction methodology.



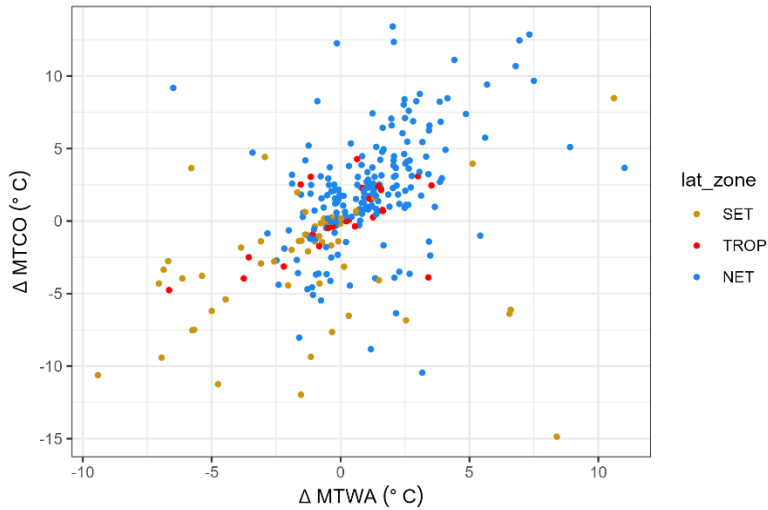
666

667

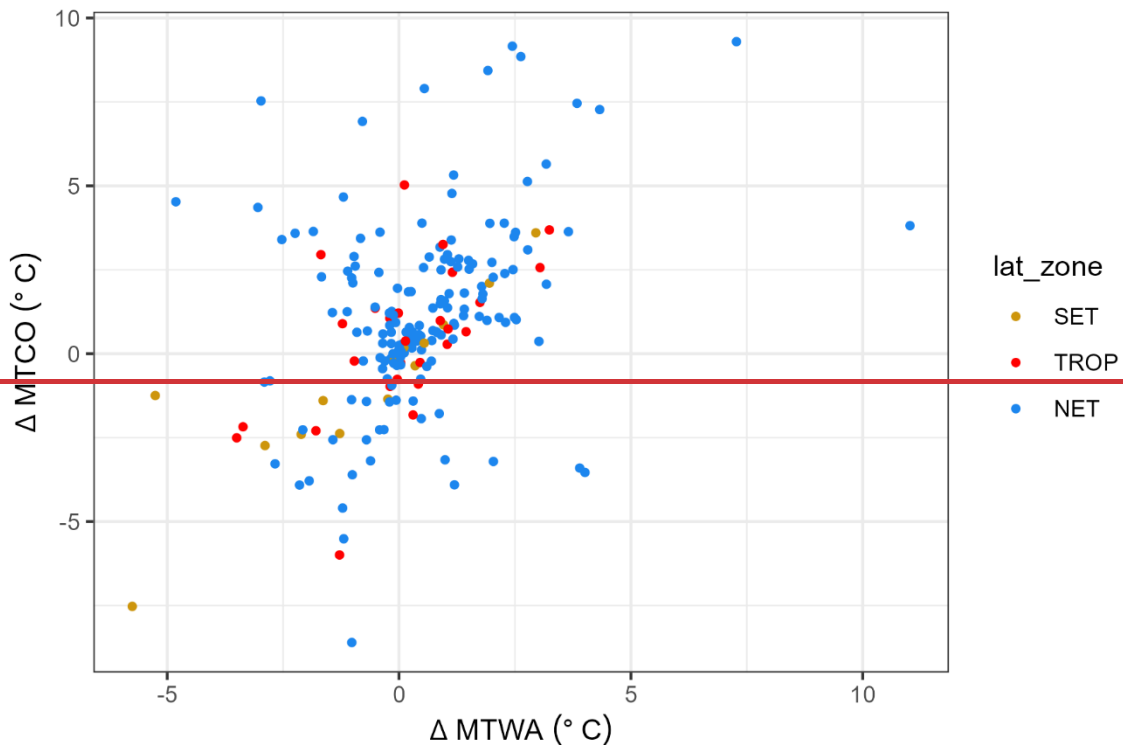
668

669

670 Figure 3: Scatter plot of the change in mean temperature of the coldest month (ΔMTCO) versus
671 the change in mean temperature of the warmest month (ΔMTWA) during individual
672 Dansgaard-Oeschger (D-O) events at individual sites. The points are colour-coded to indicate
673 whether the sites are from the northern extratropics (NET, north of 23.5°N), the tropics (TROP,
674 between 23.5°N and 23.5°S) or southern extratropics (SET, south of 23.5°S).



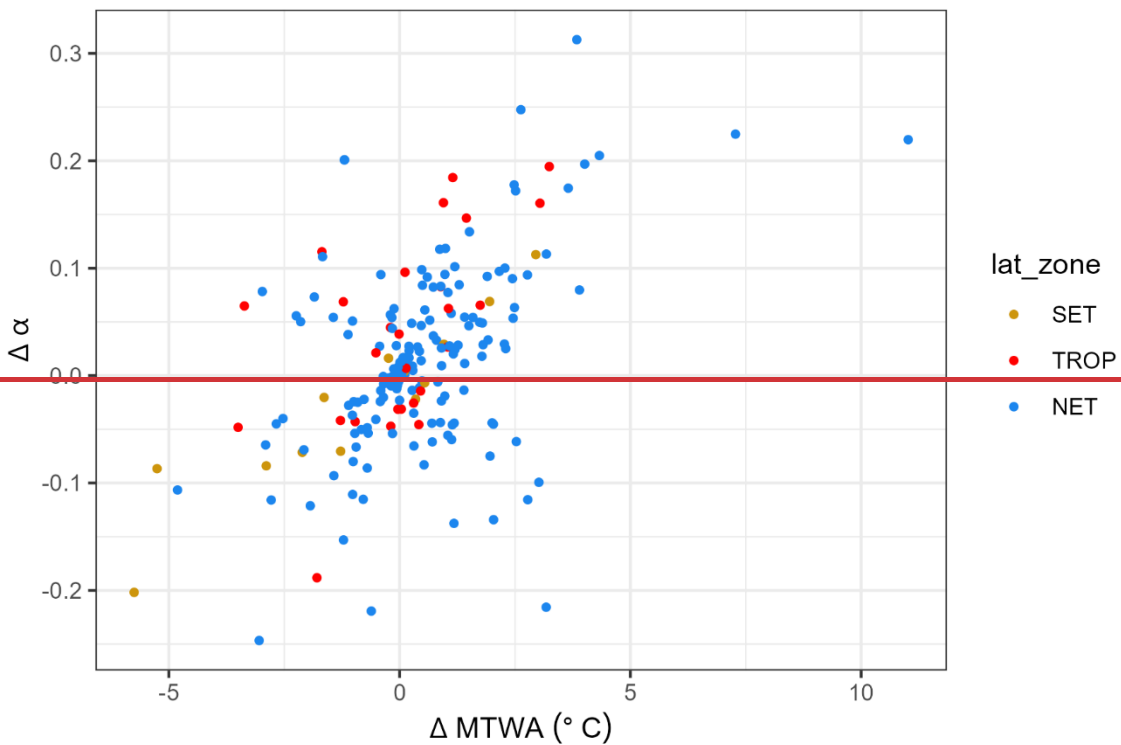
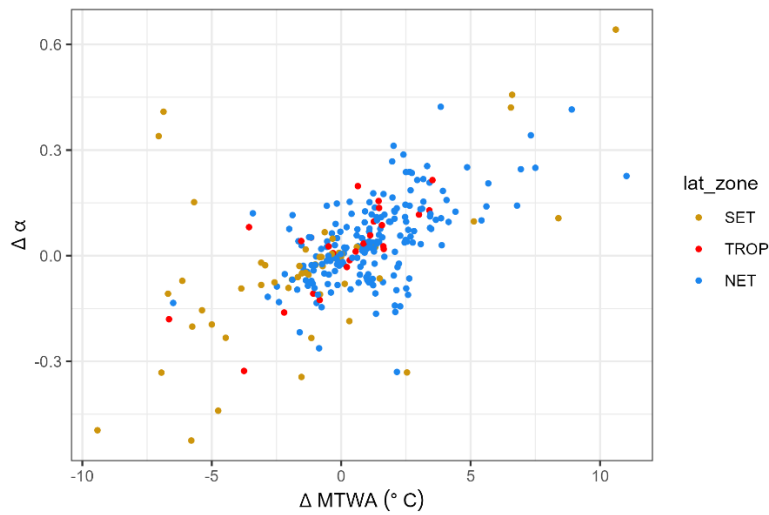
675



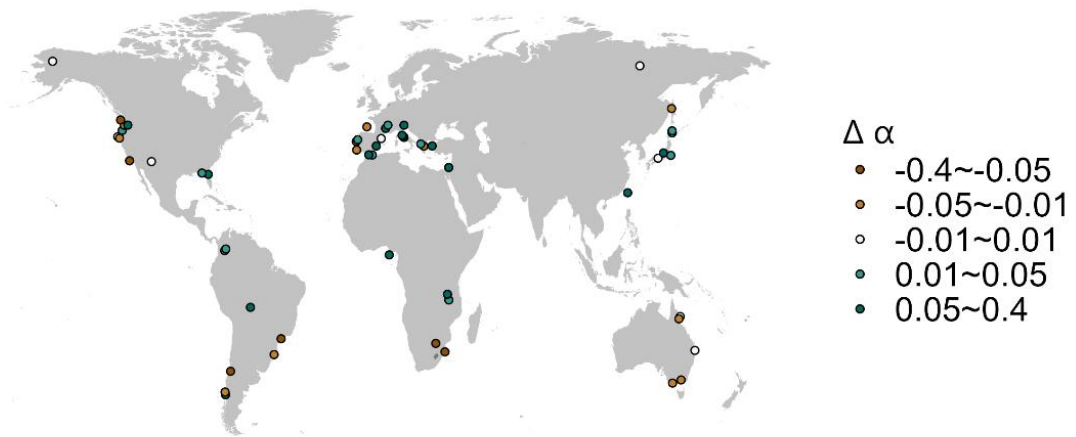
676

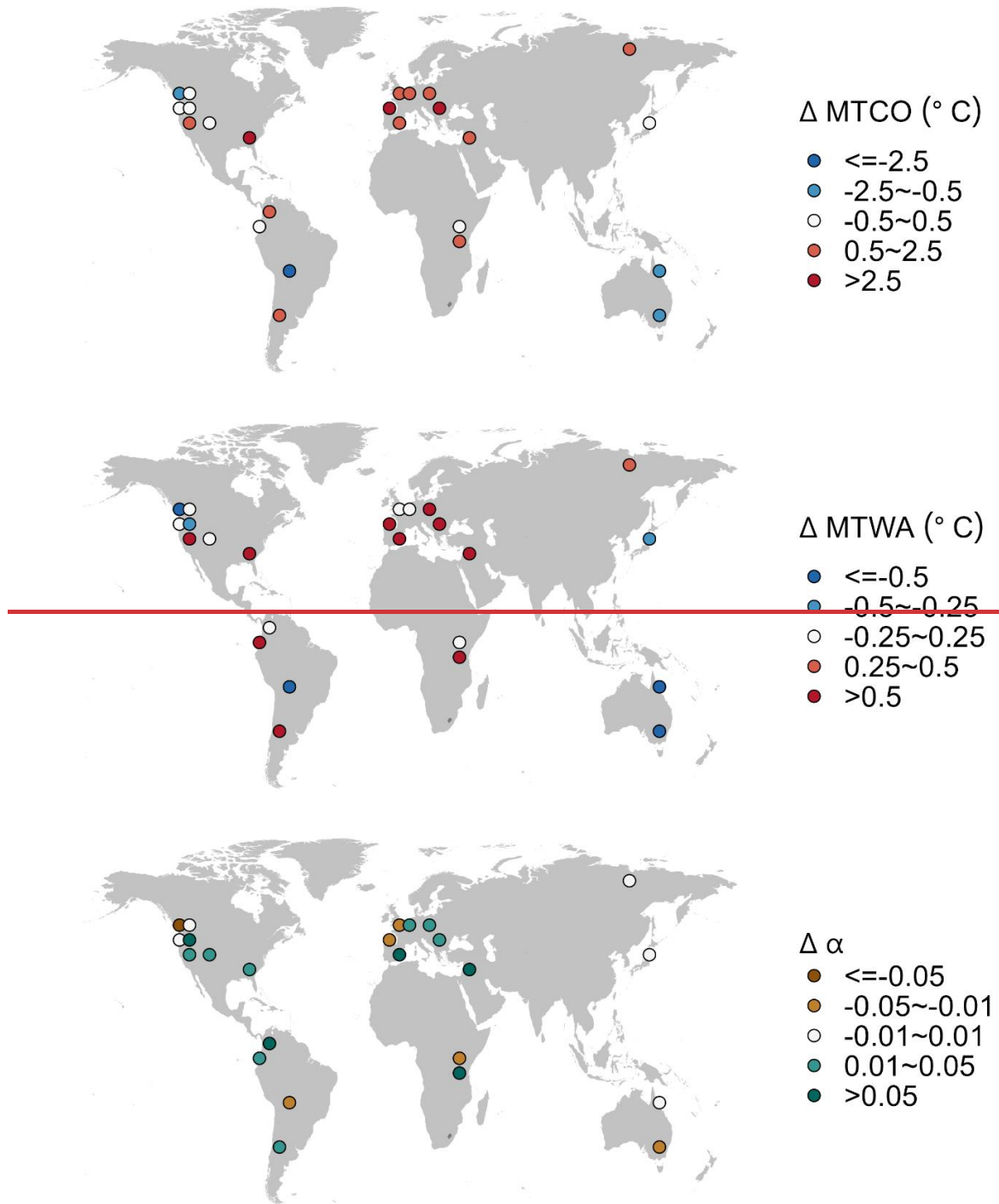
677

678 Figure 4: Scatter plot of the change in plant-available moisture ($\Delta\alpha$) versus the change in mean
679 temperature of the warmest month (ΔMTWA) during individual Dansgaard-Oeschger (D-O)
680 events at individual sites. The points are colour-coded to indicate whether the sites are from
681 the northern extratropics (NET, north of 23.5°N), the tropics (TROP, between 23.5°N and
682 23.5°S) or southern extratropics (SET, south of 23.5°S).



686 Figure 5: Maps showing the median change of site-based reconstructions for Dansgaard-
687 Oeschger (D-O) events.





689

690

691 Table 1: Details of the sites from the Abrupt Climate Changes and Environmental Responses
 692 (ACER) database (Sánchez Goñi et al., 2017) covering the interval between 50 ka and 30 ka
 693 used for the climate reconstructions. n_{due} is the number of D-O events that should be found
 694 based on the time interval covered by the record. n_{miss} is the number of D-O events that were
 695 not identified. n_{low} is the number of D-O events missed because of low resolution of part of the
 696 record. Some of the 73 sites (indicated by / in n_{due} , n_{miss} and n_{low}) provide records for parts of
 697 the 50-30ka interval but not for the intervals of the D-O events. Reconstructions based on
 698 samples where the D-O signal was not identified were not used in subsequent analyses. The
 699 full citations for each site are given in Supplementary Information.

Site-name	Latitude	Longitude	Elevation (m)	Site type	n_{due}	n_{miss}	$n_{\text{miss-low_res}}$
Abrie-Roman	41.53	1.68	350	TERR	/	/	/
Azzano-Decimo	45.88	12.72	10	TERR	8	0	0
Caledonia-Fen	-37.33	146.73	1280	TERR	/	/	/
Cambara-do-Sul	-29.05	-50.10	1040	TERR	/	/	/
Camel-Lake	30.26	-85.01	20	TERR	3	1	1
Carp-Lake	45.91	-120.88	720	TERR	8	0	0
Colnia	-23.87	-46.71	900	TERR	/	/	/
Core-Trident-163-31B	-3.61	-83.96	-3210	MARI	1	0	0
Fargher-Lake	45.88	-122.58	200	TERR	8	0	0
Framoos	47.98	9.88	662	TERR	/	/	/
Fundo-Nueva	-41.28	-73.83	66	TERR	/	/	/
Fuquene	5.45	-73.46	2540	TERR	7	1	1
GeoB3104	-3.67	-37.72	-767	MARI	/	/	/
Hay-Lake	34.00	-109.43	2780	TERR	6	1	1
Ioannina	39.75	20.85	470	TERR	8	0	0
Joe-Lake	66.77	-157.22	183	TERR	/	/	/
Kalaloch-DIGI	47.61	-124.37	19	TERR	8	0	0
Kamiyoshi-Basin (KY01)	35.10	135.59	335	TERR	1	0	0

Kashiru Bog	=3.47	29.57	2240	TERR	8	1	1
Kenbuchi Basin	44.05	142.38	135	TERR	1	1	1
Khoe	51.34	142.14	15	TERR	1	1	1
Kohuora	=36.95	174.87	5	TERR	1	1	1
Kurota Lowland	35.52	135.88	20	TERR	1	1	1
KW31	3.52	5.57	=1181	MARI	1	1	1
La-Laguna	4.92	=74.03	2900	TERR	2	0	0
Lac du Bouchet—DIGI	44.83	3.82	1200	TERR	1	1	1
Lagaceione	42.57	11.80	355	TERR	1	1	1
Laguna Bella Vista	-13.62	-61.55	600	TERR	1	1	1
Laguna Chaplin	-14.47	-61.07	600	TERR	1	1	1
Lake Billyakh	65.28	126.78	340	TERR	8	0	0
Lake Biwa (BIW95-4)	35.25	136.05	84	TERR	1	1	1
Lake Consuelo (CON1)	-13.95	-68.99	1360	TERR	1	1	1
Lake Malawi	=11.22	34.42	470	TERR	1	1	1
Lake Masoko	-9.33	33.75	840	TERR	2	0	0
Lake Nojiri	36.83	138.22	657	TERR	8	0	0
Lake Tulane	29.83	=81.95	36	TERR	1	1	1
Lake Wangoom LW87 core	=38.35	142.60	100	TERR	8	0	0
Lake Xinias	39.05	22.27	500	TERR	1	1	1
Les Echets G—DIGI	45.90	4.93	267	TERR	8	0	0
Little Lake	44.16	-123.58	217	TERR	5	0	0
Lynchs Crater	-17.37	145.70	760	TERR	8	0	0
MD01-2421	36.02	141.77	-2224	MARI	1	1	1
MD03-2622 Cariaco Basin	10.71	-65.17	-877	MARI	1	1	1
MD04-2845	45.35	=5.22	=4100	MARI	8	0	0
MD84-629	32.07	34.35	=745	MARI	8	0	0
MD95-2039	40.58	=10.35	=3381	MARI	8	0	0

MD95-2042	37.80	=10.17	=3148	MARI	+	+	+
MD95-2043	36.14	=2.62	=1841	MARI	8	0	0
MD99-2331	41.15	=9.68	=2110	MARI	8	0	0
Megali Limni	39.10	26.32	323	TERR	+	+	+
Mfabeni Peatland	=28.15	32.52	11	TERR	+	+	+
Nakafurano	43.37	142.43	173	TERR	+	+	+
Native Companion Lagoon	=27.68	153.41	20	TERR	+	+	+
Navarrs	39.10	=0.68	225	TERR	3	+	0
ODP1233-C	=41.00	=74.45	=838	MARI	+	+	+
ODP820	=16.63	146.30	=280	MARI	+	+	+
ODP-site-976	36.20	=4.30	=1108	MARI	8	0	0
ODP1019	41.66	=124.91	989	MARI	8	0	0
ODP1078C	=11.92	13.40	=426	MARI	+	+	+
ODP893A	34.28	=120.03	=577	MARI	8	0	0
Potato Lake	34.45	=111.33	2222	TERR	4	0	0
Rice Lake (Rice Lake 81)	40.30	=123.22	1100	TERR	+	+	+
Siberia	=17.09	=64.72	2920	TERR	2	0	0
Stracciaccia	42.13	12.32	220	TERR	+	+	+
Tagua-Tagua-DIGI	=34.50	=71.16	200	TERR	6	0	0
Taiquemo	=42.17	=73.60	170	TERR	+	+	+
Toushe Basin	23.82	120.88	650	TERR	+	+	+
Tswaing Crater	=25.40	28.08	1100	TERR	+	+	+
Tyrrendara Swamp	=38.20	141.76	13	TERR	+	+	+
Valle di Castiglione	41.90	12.76	44	TERR	+	+	+
W8709-13-PC	42.11	=125.75	=2712	MARI	8	0	0
W8709-8-PC	42.26	=127.68	=3111	MARI	8	+	+
Walker Lake	35.38	=111.71	2500	TERR	+	+	+

Site name	Latitude	Longitude	Elevation (m)	Site type	Reference(s)	n_{due}	n_{miss}	n_{low}
-----------	----------	-----------	---------------	-----------	--------------	-----------	------------	-----------

Abrie Romani	41.53	1.68	350	TERR	Burjachs & Ramon (1994)	2	0	0
Azzano Decimo	45.8833	12.7165	10	TERR	Pini et al. (2009)	6	2	2
Caledonia Fen	-37.3333	146.7333	1280	TERR	Kershaw et al. (2007b)	8	2	2
Cambara do Sul	-29.05	-50.1	1040	TERR	Behling et al. (2004)	7	0	0
Camel Lake	30.26	-85.01	20	TERR	Watts et al. (1992)	2	1	1
Carp Lake	45.91	-120.88	720	TERR	Whitlock and Bartlein (1997); Whitlock et al. (2000)	8	1	1
Colônia	-23.87	-46.71	900	TERR	Ledru et al. (2009)	7	4	4
Core Trident 163 31B	-3.61	-83.96	-3210	MARI	Heusser and Shackleton (1994)	/	/	/
Fargher Lake	45.88	-122.58	200	TERR	Grigg and Whitlock (2002)	8	1	1
Fundo Nueva	-41.28	-73.83	66	TERR	Heusser et al. (2000)	6	1	0
Fuquene	5.45	-73.46	2540	TERR	van Geel and van der Hammen (1973); Mommersteeg (1998)	7	2	2
Füramoos	47.98	9.88	662	TERR	Müller et al. (2003)	/	/	/
GeoB3104	-3.67	-37.72	-767	MARI	Behling et al. (2000)	/	/	/
Hay Lake	34	-109.425	2780	TERR	Jacobs (1985)	5	4	4
Ioannina	39.75	20.85	470	TERR	Tzedakis et al. (2002); Tzedakis et al. (2004)	8	1	0
Joe Lake	66.76667	-157.217	183	TERR	Anderson (1988); Anderson et al. (1994)	7	3	3
Kalaloch	47.6053	-124.371	19	TERR	Heusser (1972)	8	2	0
Kamiyoshi Basin (KY01)	35.102	135.586	335	TERR	Takahara et al. (2000);; Takahara et al. (2007); Hayashi et al. (2009)	1	0	0
Kashiru Bog	-3.47	29.57	2240	TERR	Bonnefille & Riollet (1988); Bonnefille et al. (1992)	2	2	2
Kenbuchi Basin	44.05	142.383	135	TERR	Igarashi et al. (1993); Igarashi (1996)	3	0	0
Khoe	51.341	142.14	15	TERR	Igarashi et al. (2002)	6	1	1
Kohuora	-36.95	174.8667	5	TERR	Newnham et al. (2007)	/	/	/
Kurota Lowland	35.517	135.879	20	TERR	Takahara & Kitagawa (2000)	/	/	/
KW31	3.52	5.57	-1181	MARI	Lézine & Cazet (2005); Lézine et al. (2005)	2	0	0
La Laguna	4.92	-74.03	2900	TERR	Helmens et al., (1996)	2	0	0
Lac du Bouchet	44.83	3.82	1200	TERR	Reille and de Beaulieu (1990)	8	0	0
Lagaccione	42.57	11.8	355	TERR	Magri (1999); Magri (2008)	7	2	2
Laguna Bella Vista	-13.6167	-61.55	600	TERR	Burbridge et al. (2004)	2	1	1
Laguna Chaplin	-14.4667	-61.0667	600	TERR	Burbridge et al. (2004)	1	1	1
Lake Billyakh	65.2833	126.7833	340	TERR	Müller et al. (2010)	4	0	0
Lake Biwa (BIW95-4)	35.245	136.054	84	TERR	Takemura et al. (2000); Hayashida et al. (2007); Hayashi et al. (2010)	/	/	/
Lake Consuelo (CON1)	-13.95	-68.991	1360	TERR	Urrego et al. (2005); Urrego et al. (2010)	1	1	1
Lake Malawi	-11.22	34.42	470	TERR	DeBusk (1998)	6	3	3
Lake Masoko	-9.33	33.75	840	TERR	Vincens et al. (2007)	2	0	0
Lake Nojiri	36.831	138.216	657	TERR	Kumon et al. (2009)	8	0	0

<u>Lake Tulane</u>	<u>29.83</u>	<u>-81.95</u>	<u>36</u>	<u>TERR</u>	<u>Grimm et al. (1993); Grimm et al. (2006)</u>	<u>8</u>	<u>1</u>	<u>1</u>
<u>Lake Wangoom LW87 core</u>	<u>-38.35</u>	<u>142.6</u>	<u>100</u>	<u>TERR</u>	<u>Harle et al. (2002)</u>	<u>7</u>	<u>1</u>	<u>1</u>
<u>Lake Xinias</u>	<u>39.05</u>	<u>22.27</u>	<u>500</u>	<u>TERR</u>	<u>Bottema (1979)</u>	<u>8</u>	<u>3</u>	<u>3</u>
<u>Les Echets G</u>	<u>45.9</u>	<u>4.93</u>	<u>267</u>	<u>TERR</u>	<u>de Beaulieu & Reille (1984)</u>	<u>8</u>	<u>0</u>	<u>0</u>
<u>Little Lake</u>	<u>44.16</u>	<u>-123.58</u>	<u>217</u>	<u>TERR</u>	<u>Grigg et al. (2001)</u>	<u>5</u>	<u>0</u>	<u>0</u>
<u>Lynchs Crater</u>	<u>-17.3667</u>	<u>145.7</u>	<u>760</u>	<u>TERR</u>	<u>Kershaw et al. (2007a)</u>	<u>8</u>	<u>2</u>	<u>2</u>
<u>MD01-2421</u>	<u>36.02</u>	<u>141.77</u>	<u>-2224</u>	<u>MARI</u>	<u>Igarashi & Oba (2006); Oba et al. (2006); Aoki et al. (2008)</u>	<u>7</u>	<u>2</u>	<u>0</u>
<u>MD03-2622 Cariaco Basin</u>	<u>10.7061</u>	<u>-65.1691</u>	<u>-877</u>	<u>MARI</u>	<u>González et al. (2008); González and Dupont (2009)</u>	<u>/</u>	<u>/</u>	<u>/</u>
<u>MD04-2845</u>	<u>45.35</u>	<u>-5.22</u>	<u>-4100</u>	<u>MARI</u>	<u>Sánchez Goñi et al. (2008); Daniau et al. (2009)</u>	<u>8</u>	<u>2</u>	<u>2</u>
<u>MD84-629</u>	<u>32.07</u>	<u>34.35</u>	<u>-745</u>	<u>MARI</u>	<u>Cheddadi & Rossignol- Strick (1995)</u>	<u>8</u>	<u>1</u>	<u>1</u>
<u>MD95-2039</u>	<u>40.58</u>	<u>-10.35</u>	<u>-3381</u>	<u>MARI</u>	<u>Roucoux et al. (2001); Roucoux et al. (2005)</u>	<u>8</u>	<u>0</u>	<u>0</u>
<u>MD95-2042</u>	<u>37.8</u>	<u>-10.17</u>	<u>-3148</u>	<u>MARI</u>	<u>Sánchez Goñi et al. (1999); Sánchez Goñi et al. (2000); Daniau et al. (2007); Sánchez Goñi et al. (2008); (Sánchez Goñi et al. (2009)</u>	<u>8</u>	<u>0</u>	<u>0</u>
<u>MD95-2043</u>	<u>36.14</u>	<u>-2.621</u>	<u>-1841</u>	<u>MARI</u>	<u>Sánchez Goñi et al. (2002); Fletcher and Sánchez Goñi (2008)</u>	<u>8</u>	<u>0</u>	<u>0</u>
<u>MD99-2331</u>	<u>41.15</u>	<u>-9.68</u>	<u>-2110</u>	<u>MARI</u>	<u>Sánchez Goñi et al. (2005); Naughton et al. (2007); Sánchez Goñi et al. (2008); Naughton et al. (2009)</u>	<u>8</u>	<u>1</u>	<u>1</u>
<u>Megali Limni</u>	<u>39.1025</u>	<u>26.3208</u>	<u>323</u>	<u>TERR</u>	<u>Margari et al. (2007); Margari et al. (2009)</u>	<u>6</u>	<u>1</u>	<u>0</u>
<u>Mfabeni Peatland</u>	<u>-28.1487</u>	<u>32.51867</u>	<u>11</u>	<u>TERR</u>	<u>Finch & Hill (2008)</u>	<u>5</u>	<u>1</u>	<u>1</u>
<u>Nakafurano</u>	<u>43.367</u>	<u>142.433</u>	<u>173</u>	<u>TERR</u>	<u>Igarashi et al. (1993)</u>	<u>2</u>	<u>0</u>	<u>0</u>
<u>Native Companion Lagoon</u>	<u>-27.68</u>	<u>153.41</u>	<u>20</u>	<u>TERR</u>	<u>Petherick et al. (2008a); Petherick et al. (2008b)</u>	<u>6</u>	<u>1</u>	<u>1</u>
<u>Navarrés</u>	<u>39.1</u>	<u>-0.68</u>	<u>225</u>	<u>TERR</u>	<u>Carrión & van Geel (1999)</u>	<u>3</u>	<u>1</u>	<u>0</u>
<u>ODP 1233 C</u>	<u>-41</u>	<u>-74.45</u>	<u>-838</u>	<u>MARI</u>	<u>Lamy et al. (2004); Heusser et al. (2006)</u>	<u>/</u>	<u>/</u>	<u>/</u>
<u>ODP 820</u>	<u>-16.63</u>	<u>146.3</u>	<u>-280</u>	<u>MARI</u>	<u>Moss & Kershaw (2000); Moss & Kershaw (2007)</u>	<u>7</u>	<u>3</u>	<u>3</u>
<u>ODP site 976</u>	<u>36.2</u>	<u>-4.3</u>	<u>-1108</u>	<u>MARI</u>	<u>Nebout et al. (2002); Masson-Delmotte et al. (2005)</u>	<u>8</u>	<u>1</u>	<u>0</u>
<u>ODP1019</u>	<u>41.66</u>	<u>-124.91</u>	<u>989</u>	<u>MARI</u>	<u>Mix et al. (1999); Pisias et al. (2001)</u>	<u>8</u>	<u>2</u>	<u>2</u>
<u>ODP1078C</u>	<u>-11.92</u>	<u>13.4</u>	<u>-426</u>	<u>MARI</u>	<u>Dupont & Behling (2006); Dupont et al. (2008)</u>	<u>/</u>	<u>/</u>	<u>/</u>
<u>ODP893A</u>	<u>34.28</u>	<u>-120.03</u>	<u>-577</u>	<u>MARI</u>	<u>Heusser (1998); Heusser (2000)</u>	<u>8</u>	<u>0</u>	<u>0</u>
<u>Potato Lake</u>	<u>34.45</u>	<u>-111.33</u>	<u>2222</u>	<u>TERR</u>	<u>Anderson (1993)</u>	<u>4</u>	<u>4</u>	<u>4</u>

<u>Rice Lake (Rice Lake 81)</u>	<u>40.3</u>	<u>-123.22</u>	<u>1100</u>	<u>TERR</u>	<u>L. Heusser, unpublished data</u>	<u>/</u>	<u>/</u>	<u>/</u>
<u>Siberia</u>	<u>-17.09</u>	<u>-64.72</u>	<u>2920</u>	<u>TERR</u>	<u>Mourguiart & Ledru (2003)</u>	<u>1</u>	<u>1</u>	<u>1</u>
<u>Stracciacappa</u>	<u>42.13</u>	<u>12.32</u>	<u>220</u>	<u>TERR</u>	<u>Giardini (2007)</u>	<u>5</u>	<u>1</u>	<u>1</u>
<u>Tagua Tagua</u>	<u>-34.5</u>	<u>-71.16</u>	<u>200</u>	<u>TERR</u>	<u>Heusser (1990)</u>	<u>6</u>	<u>1</u>	<u>0</u>
<u>Taiquemo</u>	<u>-42.17</u>	<u>-73.6</u>	<u>170</u>	<u>TERR</u>	<u>Heusser et al. (1999); Heusser and Heusser (2006)</u>	<u>8</u>	<u>0</u>	<u>0</u>
<u>Toushe Basin</u>	<u>23.82</u>	<u>120.88</u>	<u>650</u>	<u>TERR</u>	<u>Liew et al. (2006)</u>	<u>8</u>	<u>0</u>	<u>0</u>
<u>Tswaing Crater</u>	<u>-25.4</u>	<u>28.08</u>	<u>1100</u>	<u>TERR</u>	<u>Partridge et al. (1997); Scott et al. (2008); L. Scott, unpublished data;</u>	<u>6</u>	<u>1</u>	<u>1</u>
<u>Tyrrendara Swamp</u>	<u>-38.1986</u>	<u>141.7626</u>	<u>13</u>	<u>TERR</u>	<u>Builth et al. (2008)</u>	<u>/</u>	<u>/</u>	<u>/</u>
<u>Valle di Castiglione</u>	<u>41.9</u>	<u>12.76</u>	<u>44</u>	<u>TERR</u>	<u>Alessio et al. (1986); Follieri et al. (1988); Follieri et al. (1989); Narcisi et al. (1992); Narcisi (1999); Magri & Tzedakis (2000); Magri (2008)</u>	<u>7</u>	<u>2</u>	<u>2</u>
<u>W8709-13 PC</u>	<u>42.11</u>	<u>-125.75</u>	<u>-2712</u>	<u>MARI</u>	<u>Pisias et al. (2001)</u>	<u>7</u>	<u>2</u>	<u>2</u>
<u>W8709-8 PC</u>	<u>42.26</u>	<u>-127.68</u>	<u>-3111</u>	<u>MARI</u>	<u>Heusser (1998); Lyle et al. (1992)</u>	<u>/</u>	<u>/</u>	<u>/</u>
<u>Walker Lake</u>	<u>35.38</u>	<u>-111.71</u>	<u>2500</u>	<u>TERR</u>	<u>Berry et al. (1982); Adam et al. (1985); Hevly (1985)</u>	<u>/</u>	<u>/</u>	<u>/</u>

700

701

702 Table 2. Leave-out cross-validation (with geographically and climatically close sites removed)
 703 using fxTWA-PLSv2 for mean temperature of the coldest month (MTCO), mean temperature
 704 of the warmest month (MTWA) and plant-available water (α) with P-splines smoothed fx
 705 estimation and bins of 0.02, 0.02 and 0.002, respectively. n is the number of components where
 706 the last significant number of components is indicated in **bold**. Avg.bias is the average bias;
 707 RMSEP is the root-mean-square error of prediction; and Δ RMSEP is the per cent change of
 708 RMSEP, which is $100 \times (\text{RMSEP}_n - \text{RMSEP}_{n-1})/\text{RMSEP}_{n-1}$; when $n = 1$, RMSEP_0 is the
 709 RMSEP of the null model. p assesses whether using the current number of components is
 710 significantly different from using one component less. The degree of overall compression is
 711 assessed by linear regression of the cross-validated reconstructions on to the climate
 712 variable; b_1 and $b_{1.se}$ are the slope and the standard error of the slope, respectively. The closer
 713 the slope (b_1) is to 1, the less the compression.

	n	R^2	Avg.bias	RMSEP	Δ RMSEP	p	b_1	$b_{1.se}$
MTCO (°C)	1	0.72	-1.11	6.83	-45.45	0.001	0.83	0.00
	2	0.74	-1.21	6.68	-2.25	0.001	0.84	0.00
	3	0.75	-1.10	6.51	-2.48	0.001	0.85	0.00
	4	0.75	-1.10	6.54	0.53	1.000	0.85	0.00
	5	0.75	-1.13	6.54	-0.07	0.188	0.85	0.00
MTWA (°C)	1	0.54	-0.33	3.89	-29.76	0.001	0.66	0.00
	2	0.58	-0.32	3.69	-5.10	0.001	0.71	0.00
	3	0.59	-0.33	3.68	-0.14	0.001	0.71	0.00
	4	0.59	-0.33	3.69	0.07	0.746	0.71	0.00
	5	0.59	-0.33	3.67	-0.39	0.001	0.71	0.00
α	1	0.62	-0.02	0.189	-37.73	0.001	0.66	0.00
	2	0.63	-0.022	0.188	-0.81	0.001	0.68	0.00
	3	0.63	-0.021	0.186	-0.87	0.001	0.68	0.00
	4	0.65	-0.02	0.182	-2.11	0.001	0.71	0.00
	5	0.65	-0.02	0.182	0.11	1.000	0.71	0.00

714 Table 3: Maximum likelihood estimates of the relationship between the change in mean
 715 temperature of the coldest month (ΔMTCO) and the change in mean temperature of the
 716 warmest month (ΔMTWA) by latitudinal bands for the northern extratropics (NET, north of
 717 23.5°N), tropics (TROP, between 23.5°N and 23.5°S) and southern extratropics (SET, south of
 718 23.5°S). The intercepts were set to zero since both variables are changes. Coefficients in bold
 719 mean both the lower 95% and upper 95% estimates are above 0.

Region		Coefficient	Standard error (SE)	Lower 95%	Upper 95%
NET	Slope	<u>2.0552.129</u>	<u>0.2570.657</u>	<u>1.5510.841</u>	<u>2.5603.417</u>
TROP	Slope	<u>0.9832.276</u>	<u>0.5511.381</u>	<u>-0.098-0.431</u>	<u>2.0644.983</u>
SET	Slope	<u>1.8490.979</u>	<u>0.7720.151</u>	<u>0.3360.684</u>	<u>3.3631.275</u>

720

721

722 Table 4: Maximum likelihood estimates of the relationship between the change in plant-
 723 available water ($\Delta\alpha$) and the change in mean temperature of the warmest month (ΔMTWA) by
 724 latitudinal bands for the northern extratropics (NET, north of 23.5°N), tropics (TROP, between
 725 23.5°N and 23.5°S) and southern extratropics (SET, south of 23.5°S). The intercepts were set
 726 to zero since both variables are changes. Coefficients in bold mean both the lower 95% and
 727 upper 95% estimates are above 0.

Region		Coefficient	Standard error (SE)	Lower 95%	Upper 95%
NET	Slope	<u>0.0660.082</u>	<u>0.0090.022</u>	<u>0.0480.039</u>	<u>0.0840.124</u>
TROP	Slope	<u>0.0590.075</u>	<u>0.0200.026</u>	<u>0.0190.024</u>	<u>0.0980.127</u>
SET	Slope	<u>0.0710.031</u>	<u>0.0200.003</u>	<u>0.0320.025</u>	<u>0.1100.037</u>

728